


RESEARCH PAPER



SMURF1 controls the PPP3/calcineurin complex and TFEB at a regulatory node for lysosomal biogenesis

Qin Xia^a, Hanfei Zheng^a, Yang Li^a, Wanting Xu^a, Chengwei Wu^a, Jiachen Xu^b, Shanhu Li^c, Lingqiang Zhang^d, and Lei Dong^a 

^aKey Laboratory of Molecular Medicine and Biological Diagnosis and Treatment (Ministry of Industry and Information Technology), School of Life Science, Beijing Institute of Technology, Beijing, China; ^bState Key Laboratory of Molecular Oncology, Department of Medical Oncology, National Cancer Center/National Clinical Research Center for Cancer/Cancer Hospital, Chinese Academy of Medical Sciences & Peking Union Medical College, Beijing, China; ^cDepartment of Cell Engineering, Beijing Institute of Biotechnology, Beijing, China; ^dState Key Laboratory of Proteomics, National Center for Protein Sciences (Beijing), Beijing Institute of Lifeomics, Beijing, China

ABSTRACT

Macroautophagy/autophagy is a homeostatic process in response to multiple signaling, such as the lysosome-dependent recycling process of cellular components. Starvation-induced MTOR inactivation and PPP3/calcineurin activation were shown to promote the nuclear translocation of TFEB. However, the mechanisms via which signals from endomembrane damage are transmitted to activate PPP3/calcineurin and orchestrate autophagic responses remain unknown. This study aimed to show that autophagy regulator SMURF1 controlled TFEB nuclear import for transcriptional activation of the lysosomal biogenesis. We showed that blocking SMURF1 affected lysosomal biogenesis in response to lysosomal damage by preventing TFEB nuclear translocation. It revealed galectins recognized endolysosomal damage, and led to recruitment of SMURF1 and the PPP3/calcineurin apparatus on lysosomes. SMURF1 interacts with both LGALS3 and PPP3CB to form the LGALS3-SMURF1-PPP3/calcineurin complex. Importantly, this complex further stabilizes TFEB, thereby activating TFEB for lysosomal biogenesis. We determined that LLOme-mediated TFEB nuclear import is dependent on SMURF1 under the condition of MTORC1 inhibition. In addition, SMURF1 is required for PPP3/calcineurin activity as a positive regulator of TFEB. SMURF1 controlled the phosphatase activity of the PPP3CB by promoting the dissociation of its autoinhibitory domain (AID) from its catalytic domain (CD). Overexpression of SMURF1 showed similar effects as the constitutive activation of PPP3CB. Thus, SMURF1, which bridges environmental stress with the core autophagosomal and autolysosomal machinery, interacted with endomembrane sensor LGALS3 and phosphatase PPP3CB to control TFEB activation.

Abbreviations: ATG: autophagy-related; LLOme: L-Leucyl-L-Leucine methyl ester; ML-SA1: mucolipin synthetic agonist 1; MTOR: mechanistic target of rapamycin kinase; PPP3CB: protein phosphatase 3 catalytic subunit beta; RPS6KB1/p70S6K: ribosomal protein S6 kinase B1; SMURF1: SMAD specific E3 ubiquitin protein ligase 1; TFEB: transcription factor EB.

ARTICLE HISTORY

Received 7 November 2022
Revised 15 September 2023
Accepted 1 October 2023

KEYWORDS



Autophagy; PPP3/
Calcineurin; lysosomal
biogenesis; SMURF1; TFEB


Introduction

Macroautophagy/autophagy is a cellular homeostatic process that delivers cytoplasmic cargo to lysosomes for recycling and affects a broad range of physiological and pathological inflammation, aging, infection, immunity and cancer process [1]. This homeostatic process depends on evolutionarily conserved autophagy-related (ATG) proteins and autophagy receptors. However, the systems control autophagy in response to cellular stress or infection through interconnected mechanisms. Lysosomal calcium signaling bridges the phosphatase PPP3/calcineurin regulation and starvation-induced autophagy activation [2]. SMURF1 (SMAD specific E3 ubiquitin protein ligase 1) links selective autophagy by mediating the ubiquitylation of misfolded SOD1 (superoxide dismutase 1) and *Mycobacterium tuberculosis* to recruit autophagy machinery components [3–5]. The role of SMURF1 has been

previously considered as a cellular “selective recognition”, and little attention has been paid to the regulation of autophagy processes and the possible influence of lysosomal stress signaling.

The lysosomal biogenesis and degradation play a fundamental role in autophagic homeostasis, which is controlled by TFEB (transcription factor EB), a member of the MiT/TFE subfamily [4,6]. TFEB is retained in the cytoplasm but can translocate to the nucleus and transcript lysosomal and autophagic targets in response to diverse stresses, including lysosomal and mitochondrial damage [7,8], environmental inflammation and infection [9–11] and cancer metabolism [12]. TFEB (S211) can be phosphorylated by MTOR complex 1 (MTORC1) kinase at the lysosomal surface and then binds to YWHA (tyrosine 3-monooxygenase/tryptophan 5-monooxygenase activation protein)/14-3-3, resulting in its

CONTACT Lei Dong  ldong@bit.edu.cn  School of Life Science, Beijing Institute of Technology, 5th South Zhongguancun Street, Haidian District, Beijing 100081, China

 Supplemental data for this article can be accessed online at <https://doi.org/10.1080/15548627.2023.2267413>

© 2023 The Author(s). Published by Informa UK Limited, trading as Taylor & Francis Group.

This is an Open Access article distributed under the terms of the Creative Commons Attribution-NonCommercial-NoDerivatives License (<http://creativecommons.org/licenses/by-nc-nd/4.0/>), which permits non-commercial re-use, distribution, and reproduction in any medium, provided the original work is properly cited, and is not altered, transformed, or built upon in any way. The terms on which this article has been published allow the posting of the Accepted Manuscript in a repository by the author(s) or with their consent.

sequestration in the cytoplasm [13,14]. PPP3/calcineurin dephosphorylates TFEB, which mediates its release from YWHA/14-3-3 to drive its nuclear translocation [13]. Starvation-induced MTOR inactivation and PPP3/calcineurin activation are the common mechanisms to promote TFEB nuclear translocation [15]. Many regulatory proteins have been reported to regulate PPP3/calcineurin activity, such as RCAN (regulator of PPP3/calcineurin) [16,17], AKAP (A-kinase anchor protein), and CABIN1 (PPP3/calcineurin binding protein 1) in cardiac hypertrophy [18,19], CSNK1 (casein kinase 1) [20] and USP16 (ubiquitin specific peptidase 16) [21]. However, it is still unclear whether and how signals from endomembrane damage are transmitted to PPP3/calcineurin for its activation and to orchestrate autophagic responses.

We have previously shown that SMURF1-mediated MTORC1 signaling activation in tumor development [22]. In this study, we found that SMURF1, which bridges the environmental stress and the core autophagosomal and autolysosomal machinery, interacted with TFEB and its phosphatase PPP3CB to control the activation of TFEB.

Results

SMURF1 is required for clearance of damaged lysosomes

How can lysosomal damage be transduced to the autophagosomal system? It was reported that endomembrane injury promotes lysosomal repair and autophagy by galectins [23–25]. Additionally, both galectins and SMURF1 have been established in the clearance of *Mycobacterium tuberculosis*, which can cause endomembrane damage [26], by recruiting the components of the autophagy machinery [4,25]. However, to our knowledge, there is no literature about the possible connection between galectins and SMURF1 in response to endomembrane damage. To evaluate whether SMURF1 is involved in lysosome injury, we used the lysosomotropic compound L-Leucyl-L-Leucine methyl ester (LLOMe) to damage lysosomal membranes. We found that LLOMe (1 mM, 2 h) induced endogenous SMURF1 puncta formation (Figure 1A, quantified in B). Autophagic receptors are the best markers in degrading damaged lysosomes [27,28] as they can recognize ubiquitinated cargo for selective autophagy. Knocking down SMURF1 significantly reduced LLOMe-induced endogenous LC3 puncta compared with dimethyl sulfoxide (DMSO) treatment (Figure S1A, quantified in B). In addition, SMURF1 was indispensable for the colocalization of LC3-Ub puncta under LLOMe treatment (Figure S1C, quantified in D), indicating a link between SMURF1 and autophagy in response to lysosomal damage. Indeed, SMURF1 colocalized with LC3, SQSTM1/p62, and LAMP1 (lysosomal associated membrane protein 1, a lysosomal-specific marker) under LLOMe treatment (Figure 1C, and Figure S1E–G). The co-IP experiment also showed that SMURF1 indirectly interacts with LC3 and SQSTM1/p62 *ex vivo* (Figure 1D, E). Galectins, especially LGALS3 (galectin 3), have been widely established for damaged lysosome markers by interacting with glycans, which are present in the luminal side of the damaged lysosomal membrane, and form the

puncta upon lysosomal membrane damage [24,25]. Of note, the colocalization of Ub or LC3 with LGALS3-positive dots was also significantly blocked by knocking down SMURF1 in response to LLOMe (Figure S1H, quantified in I). These results demonstrated that SMURF1 was required for recruiting selective autophagy machinery components to damaged lysosomes.

Given that the crucial role of SMURF1 on autophagic elimination of *mycobacteria* in host defense [4] and involvement in mitophagy [29], it is of great interest to explore whether SMURF1 mediates the clearance of damaged lysosomes. We first monitored the capability of endogenous LGALS3 recruitment upon lysosomal injury. Consistently, LGALS3 dots were colocalized with LAMP1 both in SMURF1-knocked-down and parental cells upon LLOMe treatment (Figure 1F). Importantly, there was an increase of LGALS3 puncta at 1 h of LLOMe treatment in both SMURF1-knocked-down and parental cells (Figure 1F, quantified in G and H). LGALS3 profiles dispersed throughout the cells but less efficiently in SMURF1-knocked-down cells, evidenced by LGALS3 dots began to decrease and disappear at 12 h upon LLOMe washout in parental cells, but not in SMURF1-knocked-down cells (Figure 1F, quantified in G and H). These results raise the possibility that clearance of LLOMe-induced-LGALS3 dots was blocked in SMURF1-knocked-down cells. In addition, to gain insight into the effect of SMURF1 on the degradation of endogenous LGALS3, we constructed GFP-RFP-tandem fluorescence tagged LC3 (tfLC3), which GFP signals are rapidly quenched, but the RFP signals (autolysosomes) maintain relatively stable exposed to acidic lysosome. The ratio of autophagosomes (RFP⁺ GFP⁺ puncta, which is also colocalized with endogenous LGALS3 dots), to autolysosomes (RFP⁺ puncta, which is negative for LGALS3⁺ dots), significantly decreased at 8 h after LLOMe washout in parental cells. By contrast, clearance of LGALS3⁺ autophagosomes was strongly hindered in SMURF1-knocked-down cells at 8-h chase time (Figure 1I, quantified in J). To confirm autophagic degradation of LGALS3 is mediated by SMURF1, we employed tfLGALS3 as an indicator of acidity environment. The LGALS3 formed several RFP⁺GFP⁺ puncta upon LLOMe treatment, which attenuated at 6 h and abolished at 24 h after LLOMe washout in parental cells. The attenuation of GFP puncta signals was also suppressed by the autophagic inhibitor, bafilomycin A₁, which blocks the fusion of autophagosome and lysosome (Figure S1J, quantified in K). By contrast, RFP⁺ GFP⁺ puncta failed to abolish at 24 h after LLOMe washout in SMURF1-knocked-down cells (Figure S1J, quantified in K), suggesting the damaged lysosomes removed in a SMURF1-dependent manner. Consistently, we also showed that SMURF1 puncta were already detectable in the first hour of LLOMe treatment (Figure 1K), indicating SMURF1 may concert response of LGALS3-mediated ESCRT (endosomal sorting complex required for transport) complex recruitment for repairing. TRIM16 (tripartite motif-containing protein 16) coordinated recognition of membrane damage with mobilization of the core autophagy regulators in response to damaged endomembrane through the integration of LGALS3 and ubiquitin-based processes [25]. We then transfected Flag-TRIM16 in the

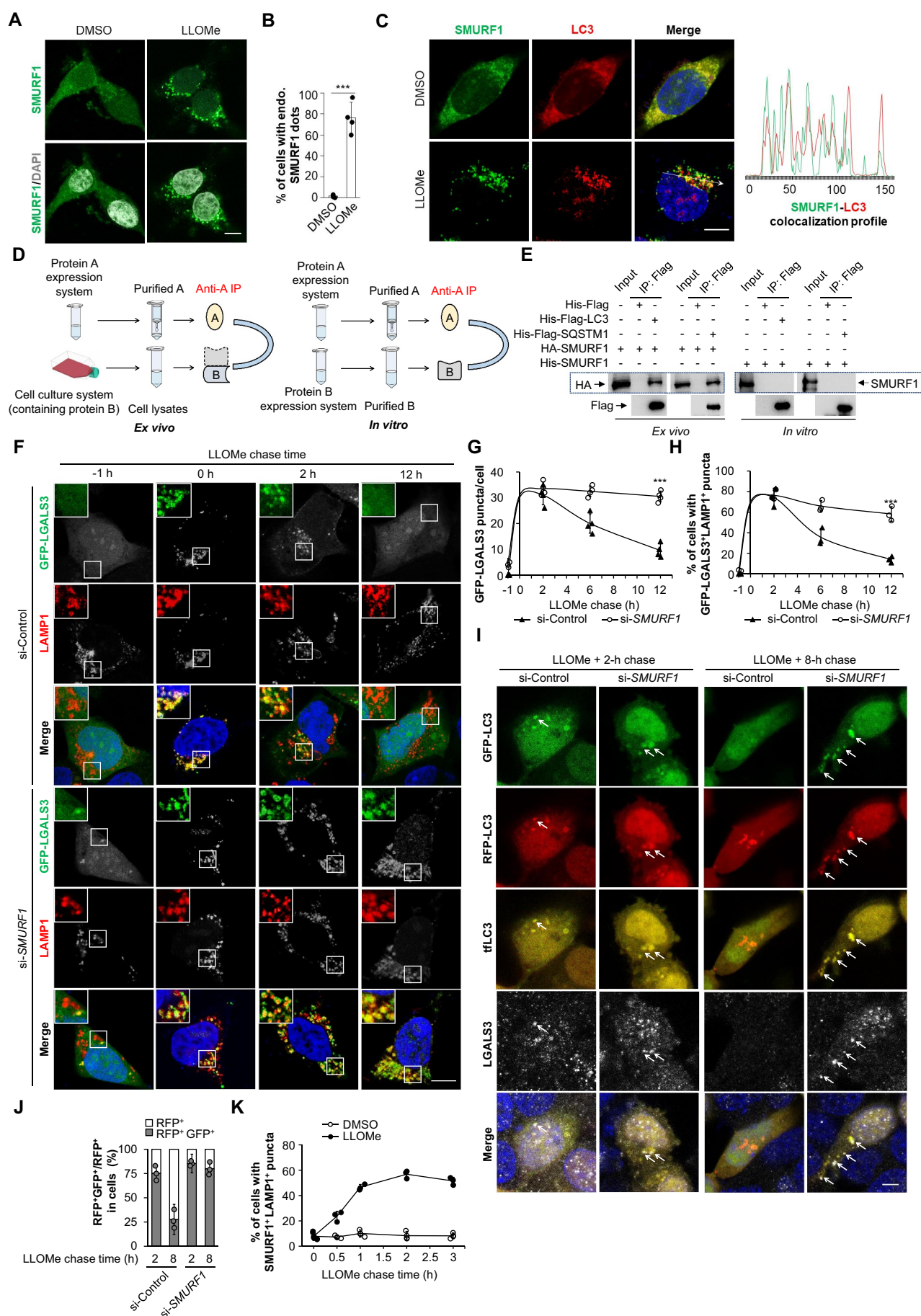


Figure 1. SMURF1 is required for the clearance of damaged lysosomes. (A and B) HEK293 cells were fixed after the treatment of LLOMe (1 mM, 2 h) or DMSO. Representative images were shown by staining with antibody against SMURF1 and DAPI (A). The quantification of the percentage of cells with endogenous SMURF1 dots was shown in (B). (C) HEK293 cells were fixed after the treatment of LLOMe (1 mM, 2 h) or DMSO, and the immunofluorescent assay was conducted by staining

HEK293 cell and conducted a GST affinity-isolation experiment. Indeed, we found the interaction of SMURF1 and TRIM16 (Figure S1L), suggesting a role of SMURF1 in cooperating with TRIM16 in response to damaged lysosomes. Altogether, these observations revealed that SMURF1 is required for the clearance of damaged lysosomes.

SMURF1 controls TFEB nuclear translocation

Given that TFEB is an established transcription factor, which links autophagy to lysosomal biogenesis [6], we wonder whether SMURF1 regulates TFEB nuclear translocation for the lysosomal clearance and biogenesis. First, to identify whether SMURF1-induced lysosomal homeostasis is dependent on TFEB, we knocked down TFEB in SMURF1-overexpressed and parental cells. We found that TFEB indeed was required for the lysosomal biogenesis, evidenced by the intensity of intact lysosome marked by LysoTracker significantly blocked by knocking down TFEB in both HA-SMURF1 and HA groups (Figure 2A, quantified in B). In addition, SMURF1 remarkably stimulated the nuclear translocation of TFEB evidenced by knocking down SMURF1 suppressed TFEB nuclear import under LLOMe treatment (Figure 2C, quantified in D). By contrast, overexpression of SMURF1 increased the nuclear portion of TFEB upon LLOMe treatment (Figure 2E, quantified in F). Moreover, subcellular fraction assay confirmed SMURF1 induced TFEB accumulation in the nucleus (Figure 2G, quantified in H). Altogether, SMURF1 promotes TFEB nuclear translocation upon endomembrane damage.

LLOMe-mediated TFEB nuclear import is dependent on SMURF1 under the condition of MTORC1 inhibition

Next, we tested whether the function of SMURF1-mediated TFEB nuclear import under LLOMe treatment is dependent on MTOR by detection of the phosphorylation level of its downstream targets. Interestingly, LLOMe prohibited the function of MTOR evidenced by decreased phosphorylation of RPS6KB1/p70S6K with or without overexpression of SMURF1 compared to control (Figure 3A), suggesting the role of SMURF1 to affect MTOR can be overridden by LLOMe response. Interestingly, we found SMURF1 suppressed significantly blocked the nuclear import of TFEB mediated by MTORC1 inhibitor torin1 compared to control cells (Figure 3B, quantified in C). Similarly, subcellular fraction assays confirmed knock-down of SMURF1 suppressed the fraction of nuclear portion of TFEB in the treatment of torin1

(Figure 3D, quantified in E), indicating SMURF1 utilizes other pathways independent of MTOR in promoting TFEB nuclear import. Yoshimori *et al.* reported that lysosomal damage (LLOMe treatment) selectively impairs the MTORC1-mediated phosphorylation of TFEB in an RRAG (Ras-related GTP binding) GTPase and ATG conjugation system-dependent manner evidenced by that LLOMe treatment reduced TFEB S211 phosphorylation and YWHA/14-3-3 binding [27,30]. Consistently, activation mutation of RRAGC^{S75L} hyperactivated TFEB phosphorylation (Figure 3F). Importantly, overexpression of SMURF1 decreased the phosphorylation of TFEB mediated by RRAGC^{S75L} (Figure 3F). Altogether, these data suggest that LLOMe-mediated TFEB nuclear import is dependent on SMURF1.

SMURF1-mediated lysosomal biogenesis is dependent on MCOLN1-PPP3/calcineurin pathway

Previous studies have shown that the subcellular localization and activity of TFEB are highly controlled by its dephosphorylated status, which is mediated by MCOLN1/mucolipin 1-PPP3/calcineurin pathway. PPP3/calcineurin is composed of a catalytic subunit, which includes PPP3CA/CNA α , PPP3CB/CNA β or PPP3CC/CNA γ , and a regulatory subunit, which includes PPP3R1/CNB α or PPP3R2/CNB β . PPP3C includes an N-terminal domain, a catalytic domain (CD), a CNB binding domain, a CALM (calmodulin)-binding domain and a C-terminal autoinhibitory domain (AID). PPP3CB is the most significant hit identified by the primary screening [2,31]. To identify whether SMURF1-mediated TFEB nuclear import is dependent on PPP3/calcineurin phosphatase activity, we found that the overexpression of constitutively active truncated mutation PPP3CB 1–474 (removed the AID), but not wild type PPP3CB, promoted TFEB nuclear import in SMURF1-knocked-down cells under LLOMe treatment (Figure 4A), suggesting that hyperactivation form of PPP3CB rescued the suppressed effect of TFEB nuclear import by knocking down SMURF1. Interestingly, we also found that the overexpression of SMURF1 had a similar effect of promoting TFEB nuclear translocation as the overexpression of constitutive activation of PPP3CB 1–474 in SMURF1-knocked-down cells during LLOMe treatment (Figure 4A, quantified in B). In addition, to identify which component of PPP3/calcineurin pathway plays a required role in the TFEB nuclear import, we suppressed key components, including MCOLN1 and PPP3CB, and checked the subcellular localization of TFEB. Cyclosporine A (CsA), a PPP3/calcineurin inhibitor, blocked

with anti-LC3 and anti-SMURF1 antibodies instead. The nucleus was stained by DAPI (left). Fluorescence peaks and colocalization profile of LC3 and SMURF1 (LLOMe, 2 h) were illustrated by line tracers (right). (D and E) Schematic diagram of *ex vivo* and *in vitro*. *Ex vivo* IP: the immunoprecipitation with purified protein A in the bacteria expression system and the cell lysates containing protein B in the cell culture was conducted to verify the indirect interaction between protein A and protein B; *in vitro* IP: the immunoprecipitation with purified protein A and protein B in the bacteria expression system respectively was conducted to verify the direct interaction (D). Co-immunoprecipitation (co-IP) assay analysis of the interaction between SMURF1 and LC3 or SQSTM1/p62. His-Flag-LC3 or His-Flag-SQSTM1/p62 purified from *E. coli* was conducted to interact with HA-SMURF1 transfected in HEK293 cells (*ex vivo*) or His-SMURF1 purified from *E. coli* (*in vitro*) (E). (F–H) HEK293 cells were transfected with SMURF1 or scramble siRNA oligos for 48 h and transfected with GFP-LGALS3 for another 24 h. Cells were fixed at 1 h with or without treatment of LLOMe (1 mM) and at 2 h or 12 h of washout. Cells were stained with DAPI and antibody against LAMP1 (F). The number of GFP-LGALS3 puncta per cell was shown in (G) and the percentage of cells containing GFP-LGALS3⁺ LAMP1⁺ puncta was shown in (H). (I and J) HEK293 cells were transfected with SMURF1 or scramble siRNA oligos for 48 h and transfected with tflc3 for another 24 h. Cells were then treated with LLOMe (1 mM) for 1 h and chased for 2 h and 8 h. The nucleus was stained by DAPI. Immunofluorescence was analyzed by staining with antibody against LGALS3 (I), and the percentage of RFP⁺ GFP⁺/RFP⁺ puncta was quantified (J). (K) The percentage of cells containing SMURF1⁺ LAMP1⁺ puncta was shown in response to LLOMe or DMSO at different chase times. Scale bar: 5 μ m; $n \geq 50$ cells per group. Data were from three independent experiments represented as means \pm SEM. *** $p < 0.001$.

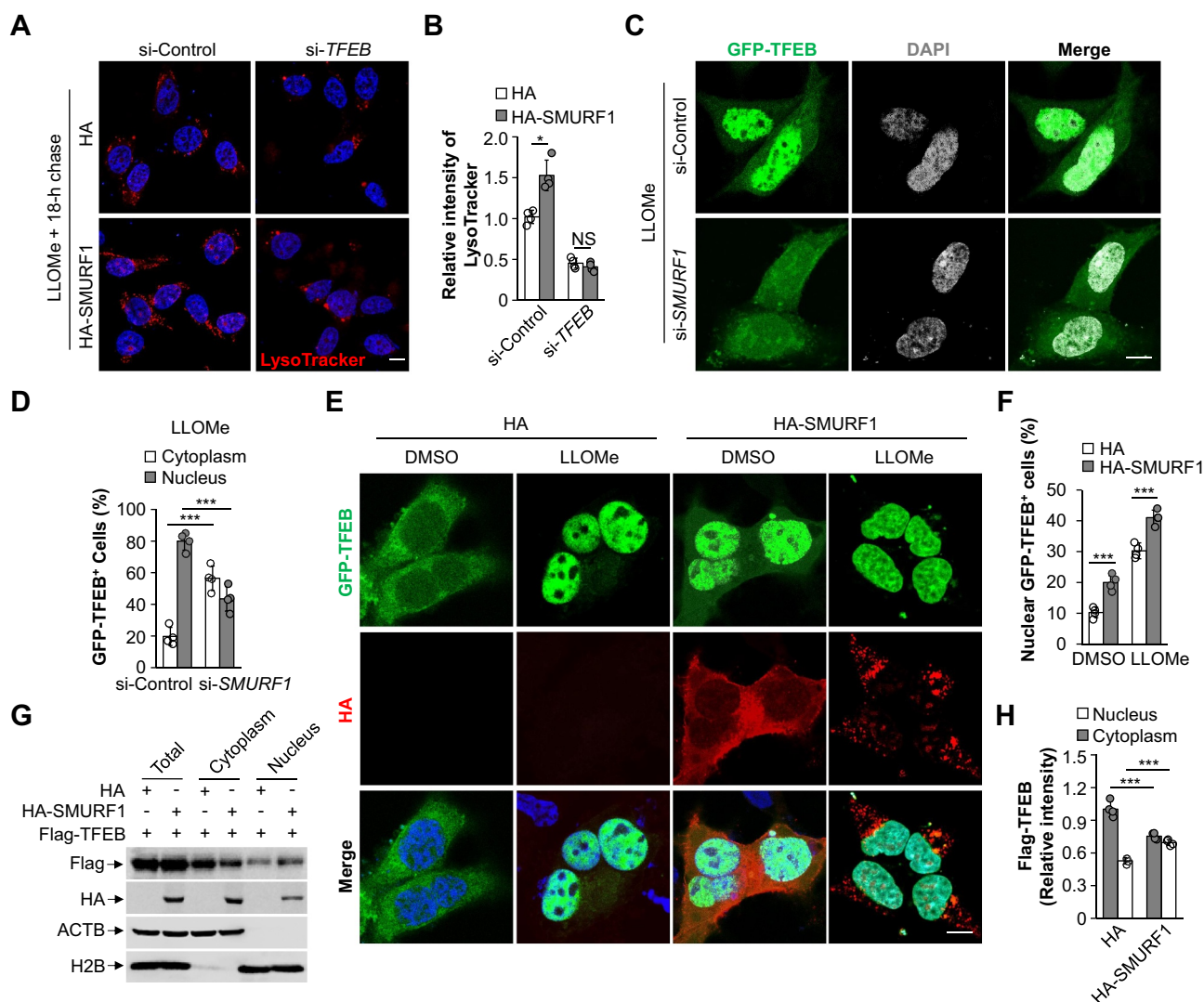


Figure 2. SMURF1 controls TFEB nuclear translocation. (A and B) HEK293 cells were transfected with siRNA against *TFEB*. After 48 h, cells were re-transfected with HA or HA-SMURF1 for another 24 h and chased for 18 h after LLOMe (1 mM, 1 h) washout, and then stained with LysoTracker and Hoechst (A). The quantification of LysoTracker's relative intensity per cell is shown in (B). (C and D) HEK293 cells were transfected with *SMURF1* or scramble siRNA oligos for 48 h, then transfected with GFP-TFEB for another 24 h. Cells were then fixed and stained with DAPI after the treatment of LLOMe (1 mM, 2 h) and visualized using confocal microscopy (C). The percentage of cells with GFP-TFEB in cytoplasm or nucleus respectively are shown in (D). (E and F) HEK293 cells were transfected with GFP-TFEB and HA or HA-SMURF1 for 24 h, and were treated with LLOMe (1 mM, 2 h) or DMSO before fixation and stained with DAPI and HA antibody (E). The percentage of cells with GFP-TFEB in nucleus is shown in (F). (G and H) HEK293 cells were transfected with Flag-TFEB with HA or HA-SMURF1 for 24 h, and then cells were harvested and carried out nuclear and cytoplasmic separation assay, and lysates were subjected to western blotting analysis using anti-Flag, anti-HA, anti-ACTB/ β -actin and anti-H2B/histone 2B antibodies (G). The percentage of cells with Flag-TFEB in cytoplasm and nucleus are respectively shown in (H). Scale bar: 5 μ m; $n \geq 50$ cells per group. Data were from three independent experiments represented as means \pm SEM. NS $p > 0.05$; * $p < 0.05$; *** $p < 0.001$.

SMURF1-induced TFEB nuclear translocation (Figure 4C, quantified in D). Importantly, subcellular cytoplasmic and nuclear assay verified that knocking down PPP3CB or MCOLN1 significantly blocked TFEB nuclear import mediated by overexpressed SMURF1 (Figure 4E, F, quantified in G). Whether lysosomal calcium efflux triggers SMURF1-PPP3/calineurin system-dependent TFEB activation remains unknown. Consistent with this notion, SMURF1-knocked-down cells exhibited impaired TFEB nuclear translocation following an agonist for the lysosomal calcium channel MCOLN1, mucolipin synthetic agonist 1 (ML-SA1) treatment in response to LLOMe (Figure S2A), indicating agonist of MCOLN1 cannot override the silencing of SMURF1 during LLOMe treatment. Conversely, TFEB nuclear translocation by overexpression of SMURF1 in response to LLOMe was impaired in the cells

treated with BAPTA-AM, which chelates intracellular calcium (Figure S2A), suggesting that SMURF1-mediated TFEB activation is dependent on lysosomal calcium efflux. In addition, overexpression of SMURF1 followed by ML-SA1, without the LLOMe, also failed to recruit SMURF1 to lysosome (Figure S2B), suggesting calcium efflux alone cannot recruit SMURF1. Consistently, we also found that calcium-dependent process was triggered by LLOMe, evidenced by that calcium chelators BAPTA-AM significantly blocked SMURF1 recruitment (Figure 4H).

LGALS3 recruits SMURF1 and PPP3CB

Previously, it has been reported that lysosomal integrity is monitored by LGALS8 (galectin 8), which recruits

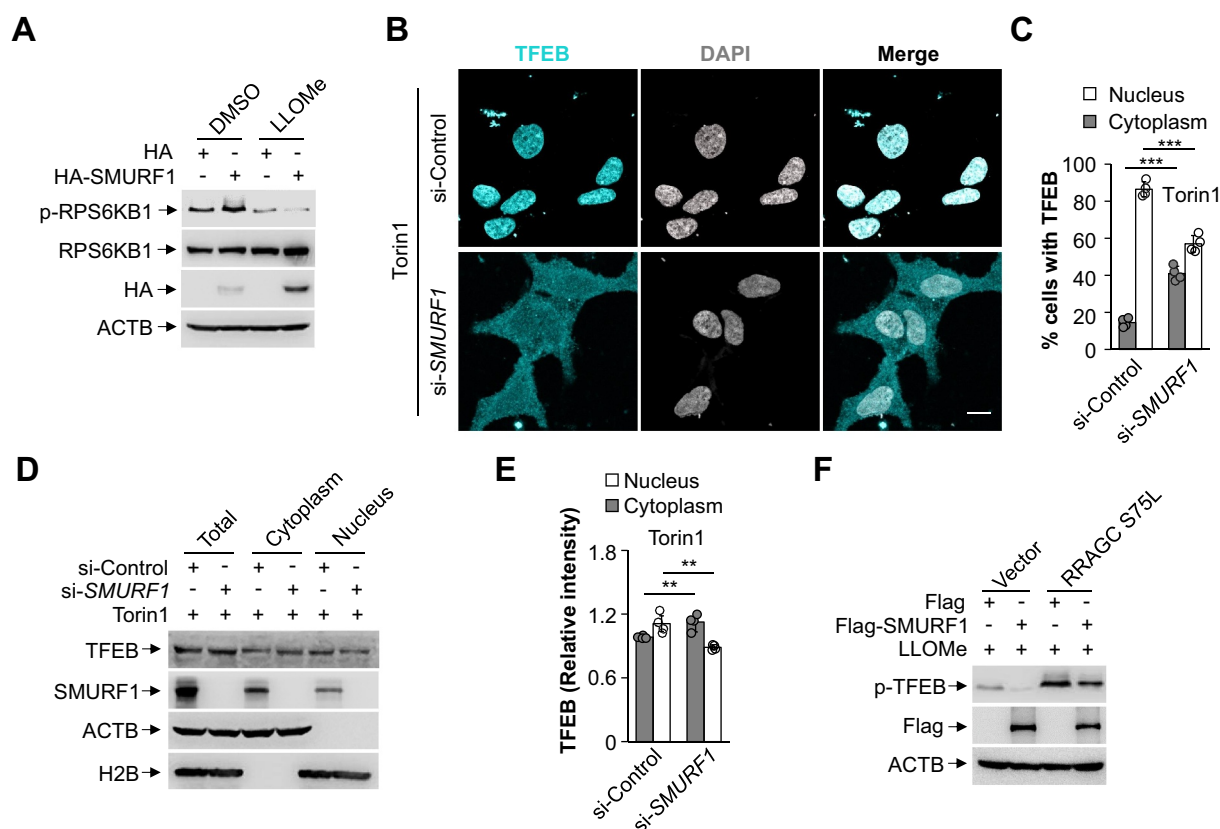


Figure 3. Lome-mediated TFEB nuclear import is dependent on SMURF1 under the condition of MTORC1 inhibition. (A) HEK293 cells were transfected with HA or HA-SMURF1 for 24 h, and then were treated with LLOMe (1 mM, 2 h) and equal volume DMSO. Cells were subjected to western blotting using p-RPS6KB1/p-p70S6K, RPS6KB1/p70S6K, HA and ACTB/ β -actin antibodies. (B and C) HEK293 cells were transfected with *SMURF1* or scramble siRNA oligos for 72 h. Cells were treated with torin1 (250 nM) for 1 h before fixation and staining with TFEB antibody and DAPI (B). The percentage of cells with TFEB in cytoplasm and nucleus are respectively shown in (C). (D and E) HEK293 cells were transfected with *SMURF1* or scramble siRNA oligos for 72 h and then treated with torin1 (250 nM) for 1 h. Cells were subjected to nuclear and cytoplasmic separation assay and western blotting analysis using anti-TFEB, anti-SMURF1, anti-ACTB/ β -actin and anti-H2B/histone 2B antibodies (D). The relative intensity of TFEB in cytoplasm and nucleus are shown in (E). (F) HEK293 cells were transfected with Flag or Flag-SMURF1 for 12 h, and then cells were transfected with HA-GST (vector) or HA-GST-RRAGC^{S75L} for another 12 h. Cells were then treated with LLOMe (1 mM, 2 h) and subjected to western blotting using Flag, p-TFEB and ACTB/ β -actin antibodies. Scale bar: 5 μ m; $n \geq 50$ cells per group. Data were from three independent experiments represented as means \pm SEM. ** $p < 0.01$; *** $p < 0.001$.

CALCOCO2/NDP52 (calcium binding and coiled-coil domain 2) to activate antibacterial autophagy [32]. Further study also establishes that LGALS8 inhibits MTOR in response to lysosomal injury [23]. Additionally, endomembrane exposure leads to LGALS3 recruiting ESCRT components to damaged lysosomes to repair [24]. To determine whether SMURF1 recruited to the lysosome is directly dependent on endomembrane damage-modulated galectins, immunofluorescence assays were conducted to identify whether SMURF1 associated with galectins exposed to LLOMe. It showed that LGALS3 was required for the recruitment of SMURF1 to damaged lysosome evidenced by loss of LGALS3, but not LGALS8, significantly reduced the colocalization of SMURF1 and LAMP1 in response to LLOMe (Figure S3A). Importantly, SMURF1 was colocalized with LGALS3 and LAMP2 (lysosomal-associated membrane protein 2) (Figure 5A), suggesting SMURF1 could be recruited by LGALS3. Indeed, both *in vitro* and *ex vivo* assays revealed that SMURF1 indirectly bound to LGALS3, but not LGALS8, in LLOMe-enhanced and E3 ligase activity-independent manner (Figure 5B, Figure S3B-D). Our data also showed that SMURF1 was not able to ubiquitylate LGALS3 (Figure S3E).

Next, we mapped the specific LGALS3 (containing non-lectin N-terminal domain: NT and carbohydrate recognition domain: CRD) and SMURF1 (containing C2, WW and HECT domains) interaction domain by constructing truncated LGALS3 and SMURF1 as indicated in Figure 5C. We found LGALS3 NT domain and SMURF1 C2 domain were required for their indirect interaction *ex vivo* (Figure 5D, E). To examine whether PPP3CB could bridge the interaction between LGALS3 and SMURF1, we first overexpressed SMURF1 and PPP3CB with or without knock-down of LGALS3. It showed that LGALS3 was required for PPP3CB recruitment (Figure 5A). By mapping the binding domain of LGALS3 and PPP3CB, our data revealed that their interaction was dependent on the N-term domain (1–21 amino acid) of PPP3CB and the CRD domain of LGALS3 (Figure 5F, G, H, Figure S3F-I). Previous studies show that PPP3CB^{P14G, P18G} point mutation and PPP3CB 22–525 truncated mutation from the proline-rich sequence of the N-term domain are involved in substrate recognition [33]. Indeed, we verified that PPP3CB^{P14G, P18G} mutation no longer interacted with LGALS3 (Figure 5I, Figure S3J). It is also reported that the LxVP and PxIxIT motifs can recognize and bind to PPP3/

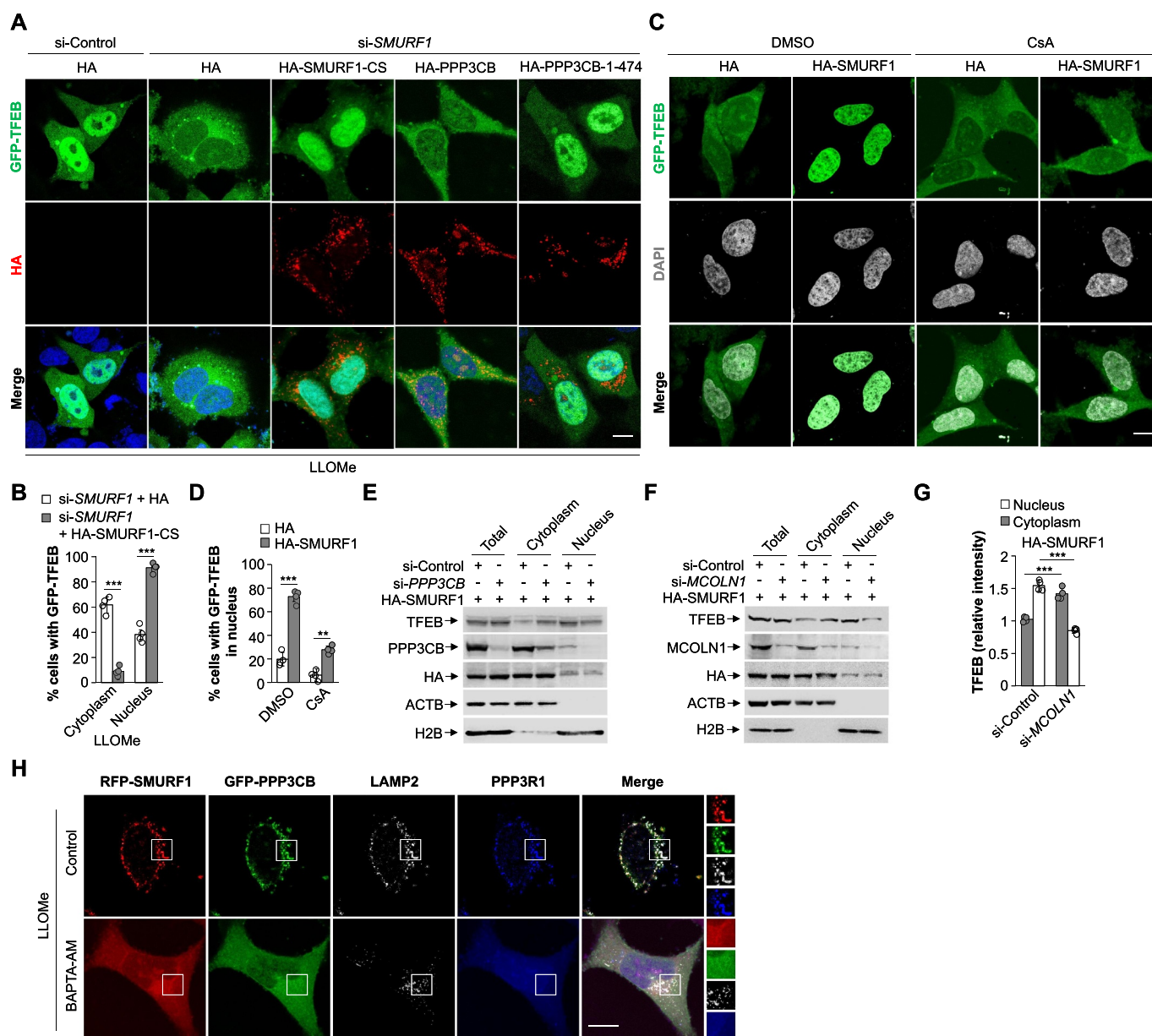


Figure 4. SMURF1-mediated lysosomal biogenesis is dependent on MCOLN1-PPP3/calcineurin pathway. (A and B) HEK293 cells were transfected with *SMURF1* or scramble siRNA oligos. After 48 h, cells were transfected with GFP-TFEB and HA or HA-SMURF1-CS or HA-PPP3CB or HA-PPP3CB 1–474 for another 24 h. Cells were fixed and stained with DAPI and HA antibody after LLOMe (1 mM, 2 h) treatment (A). The percentage of cells with GFP-TFEB in cytoplasm and nucleus are respectively shown in (B). (C and D) HEK293 cells were transfected with GFP-TFEB and HA or HA-SMURF1, and treated with CsA (2 μ M) for 4 h before fixation and stained with DAPI (C). The percentage of cells with GFP-TFEB in nucleus is shown in (D). (E–G) HEK293 cells were transfected with *PPP3CB* or *MCOLN1* or scramble siRNA oligos for 48 h and transfected with HA-SMURF1 for another 24 h. Cells were subjected to nuclear and cytoplasmic separation assay and western blotting analysis using anti-TFEB, anti-PPP3CB, anti-MCOLN1, anti-HA, anti-ACTB/ β -actin and anti-H2B/histone 2B antibodies (E and F). The relative intensity of TFEB in cytoplasm and nucleus in (F) are shown in (G). (H) HEK293 cells were transfected with RFP-SMURF1 and GFP-PPP3CB for 24 h. Cells were treated with or without BAPTA-AM (25 μ M, 1 h) and LLOMe (1 mM) for 2 h. Cells were then fixed and stained with DAPI. Immunofluorescent assay was conducted by staining with LAMP2 and PPP3R1 antibodies. Scale bar: 5 μ m; $n \geq 50$ cells per group. Data were from three independent experiments represented as means \pm SEM. ** $p < 0.01$; *** $p < 0.001$.

calcineurin [34]. Therefore, we analyzed and found LGALS3 sequence contains the LIVP motif, which is located at the amino acids 114–117 of the CRD domain. We then deleted the LIVP motif from LGALS3, and found no interactions were observed between PPP3CB and LGALS3 Δ LIVP (Figure 5J), suggesting LGALS3 LIVP motif is required for its interaction with PPP3CB. Altogether, PPP3CB might interconnectedly bridge the formation of LGALS3-SMURF1-PPP3CB complex (Figure 5K).

SMURF1 promotes the capability of LGALS3 to recruit PPP3R1

Immunofluorescence assay showed that PPP3R1 was also recruited to lysosomes upon LLOMe treatment in a LGALS3-dependent manner (Figure S4A). To identify the role of PPP3R1 in the formation of complex, as expected, we first found that PPP3CB directly binds with PPP3R1 in a LLOMe-enhanced manner (Figure 6A, B). Considering that

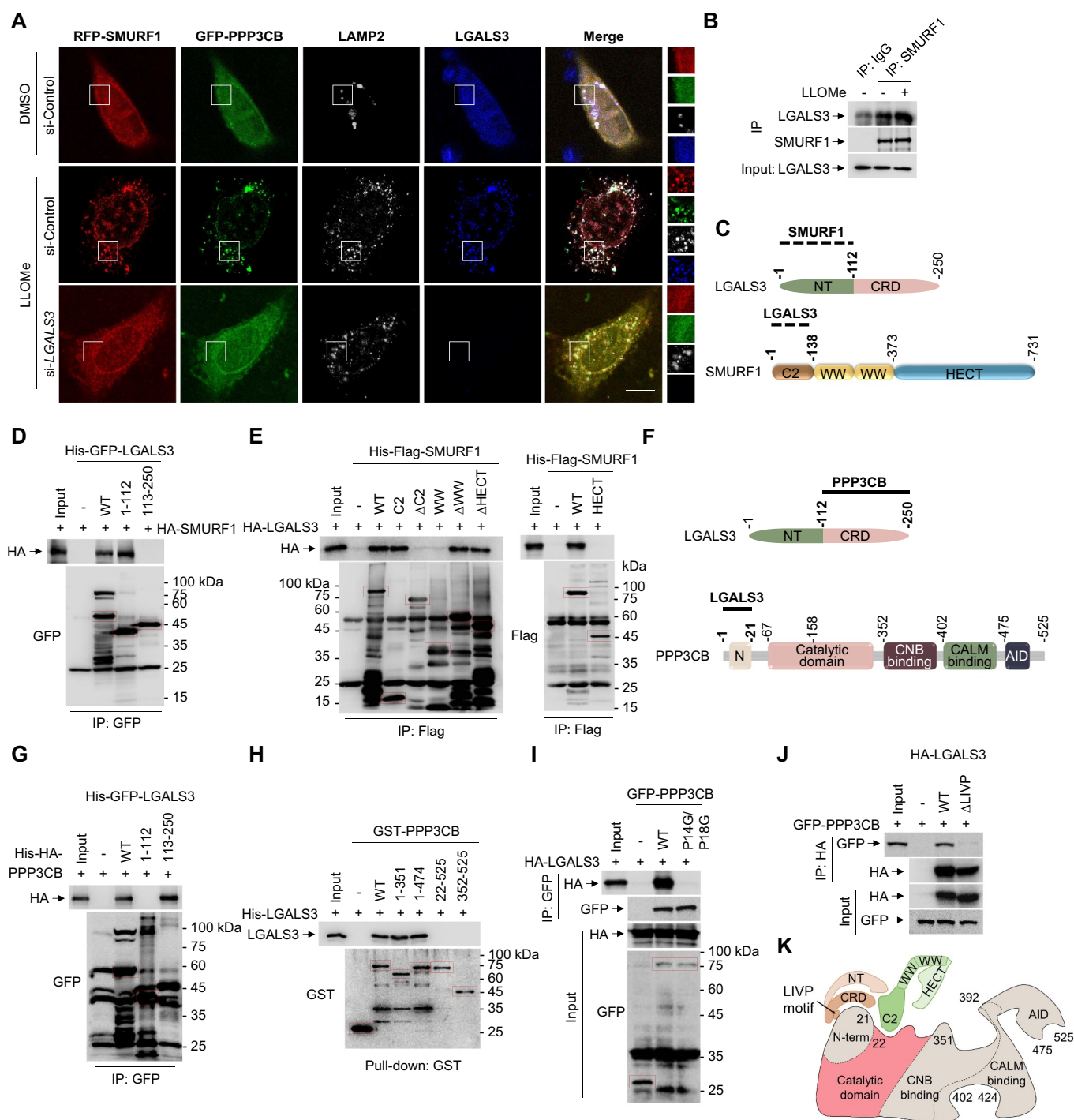


Figure 5. LGALS3 recruits SMURF1 and PPP3CB. (A) HEK293 cells were transfected with *LGALS3* or scramble siRNA oligos for 48 h, and then overexpressed with RFP-SMURF1 and GFP-PPP3CB for another 24 h. Cells were fixed at 2 h after the treatment of LLOMe (1 mM) or DMSO. Immunofluorescent assay was conducted by staining with antibodies against LAMP2 and LGALS3. (B) Co-IP assay analysis of the indirect association of endogenous SMURF1 and LGALS3 of HEK293 cells after the treatment of LLOMe (1 mM, 2 h) or DMSO. (C) Schematic diagram of mapping the indirect interaction between LGALS3 and SMURF1. (D) Co-IP analysis of the interaction between HA-SMURF1 expressed in HEK293 cells and His-GFP-LGALS3 constructs purified from *E. coli*. (E) Co-IP analysis of the interaction between HA-LGALS3 expressed in HEK293 cells and His-Flag-SMURF1 constructs purified from *E. coli*. (F) Schematic diagram of mapping the direct interaction between LGALS3 and PPP3CB. (G) Co-IP analysis of the interaction between His-HA-PPP3CB and His-GFP-LGALS3 constructs purified from *E. coli*. (H) Affinity-isolation analysis of the direct interaction between His-LGALS3 and GST-PPP3CB constructs purified from *E. coli*. (I) Co-IP analysis of the interaction between HA-LGALS3 and GFP-PPP3CB (or GFP-PPP3CB^{P14G, P18G}) expressed in HEK293 cells. (J) Co-IP analysis of the interaction between GFP-PPP3CB and HA-LGALS3 (or HA-LGALS3^{ΔLIVP}) expressed in HEK293 cells. (K) Schematic diagram of LGALS3 interacts with SMURF1 and PPP3CB. Scale bar: 5 μ m. Data were representative of three independent experiments.

PPP3CB was directly associated with LGALS3, we also checked the interaction between PPP3R1 and LGALS3. The results showed that PPP3R1 indirectly binds with LGALS3 (Figure 6C). Similarly, LLOMe treatment also promoted the

binding affinity between PPP3R1 and LGALS3 (Figure 6D). We next mapped the key interaction domain of LGALS3 with PPP3R1, and showed the NT domain of LGALS3 was essential for the association with PPP3R1 (Figure 6E, F).

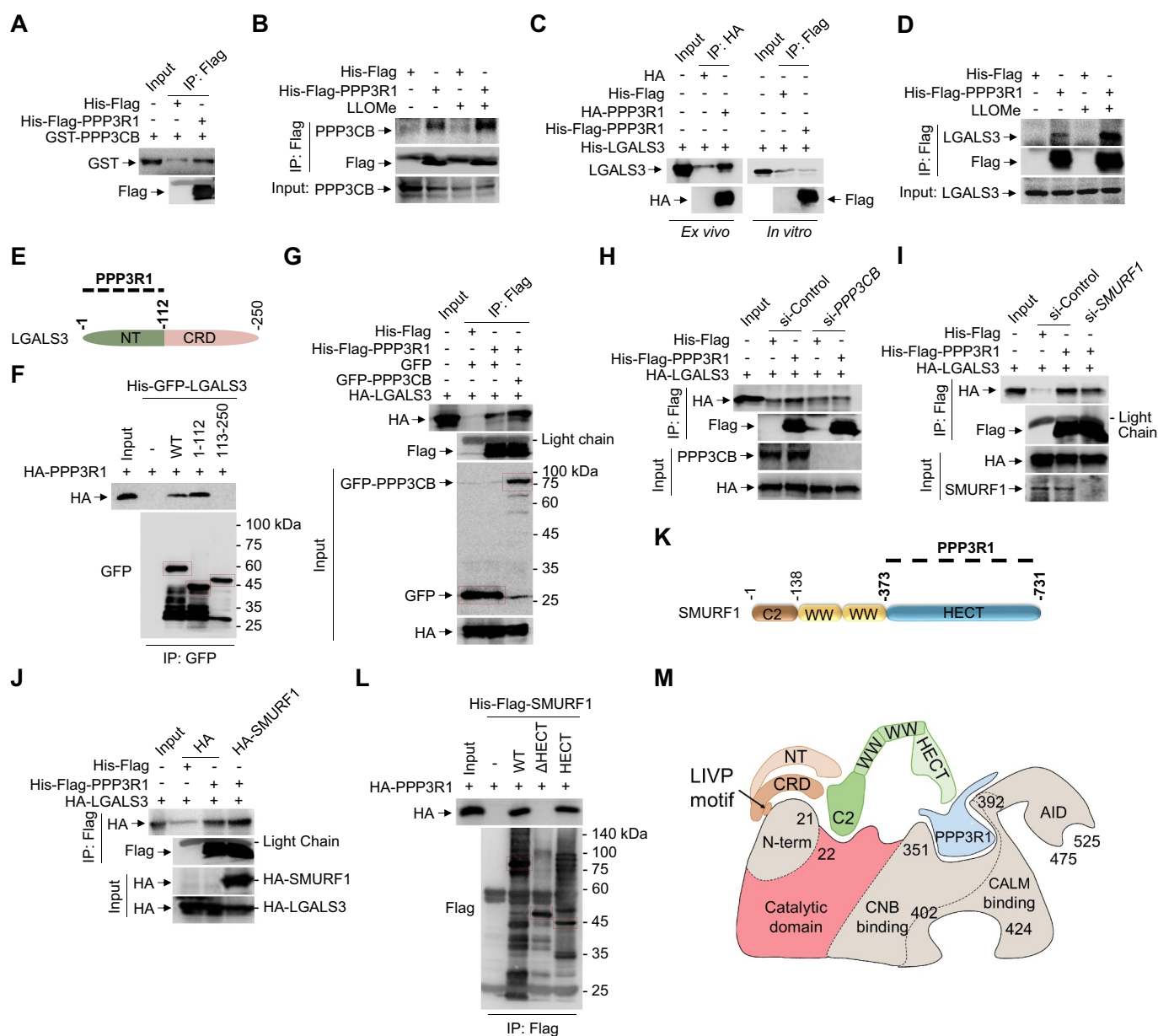


Figure 6. SMURF1 promotes the capability of LGALS3 to recruit PPP3R1. (A) Co-IP analysis of the direct association between GST-PPP3CB and His-Flag-PPP3R1 purified from *E. coli*. (B) HEK293 cell lysates were collected after LLOMe (1 mM, 2 h) treatment. Co-IP analysis of the indirect interaction between endogenous PPP3CB and His-Flag-PPP3R1 purified from *E. coli*. (C) Co-IP assay analysis of the association between PPP3R1 and LGALS3. His-LGALS3 purified from *E. coli* was conducted to interact with HA-PPP3R1 transfected in HEK293 cells (*ex vivo*) or His-Flag-PPP3R1 purified from *E. coli* (*in vitro*). (D) HEK293 cell lysates were collected after LLOMe (1 mM, 2 h) treatment. Co-IP analysis of the indirect interaction between endogenous LGALS3 and His-Flag-PPP3R1 purified from *E. coli*. (E) Schematic diagram of mapping the indirect interaction between LGALS3 and PPP3R1. (F) HEK293 cells were transfected with HA-PPP3R1 for 24 h. Co-IP analysis of the indirect interaction between HA-PPP3R1 and/or His-GFP-LGALS3 constructs purified from *E. coli*. (G) HA-LGALS3-overexpressed HEK293 cells were transfected with GFP-PPP3CB or GFP for 24 h. Co-IP analysis of the indirect interaction between HA-LGALS3 and His-Flag-PPP3R1 purified from *E. coli*. (H-J) HEK293 cells were transfected with or without si-PPP3CB (H), si-SMURF1 (I), or HA-SMURF1 (J) and then overexpressed with HA-LGALS3. Co-IP analysis of the indirect interaction between HA-LGALS3 and His-Flag-PPP3R1 purified from *E. coli*. (K) Schematic diagram of mapping the indirect interaction between SMURF1 and PPP3R1. (L) HEK293 cells were transfected with HA-PPP3R1 for 24 h. Co-IP analysis of the indirect interaction between HA-PPP3R1 and His-Flag-SMURF1 constructs purified from *E. coli*. (M) Schematic diagram of SMURF1 promotes LGALS3 recruitment of PPP3R1. Data were representative of three independent experiments.

Furthermore, overexpression of PPP3CB increased, suppression of PPP3CB abolished, the interactions of PPP3R1 and LGALS3 (Figure 6G, H), suggesting PPP3CB is also the bridge for the interaction between LGALS3 and PPP3R1. Interestingly, we also detected that SMURF1 indirectly interacted with PPP3R1, but not MCOLN1, in a LLOMe-

enhanced manner (Figure S4B-E). Given that both SMURF1 and PPP3R1 were indirectly bound with the NT domain of LGALS3, we asked whether SMURF1 affected the interactions between PPP3R1 and LGALS3. Our data indicated that suppression of SMURF1 decreased, overexpression of SMURF1 increased, the interactions of PPP3R1 and

LGALS3 (Figure 6I, J), suggesting SMURF1 promotes the recruitment of PPP3R1 by LGALS3. We next mapped the key HECT domain of SMURF1 which was essential for interaction with PPP3R1 (Figure 6K, L). Altogether, SMURF1-enhanced recruitment of PPP3R1 was dependent on PPP3CB (Figure 6M).

SMURF1 promotes PPP3CB CD and AID disassociation

What role does SMURF1 play in the LGALS3-PPP3/calci-neurin complex? To begin with, we tested whether SMURF1 could directly bind to PPP3CB. As expected, we identified that SMURF1 directly bound PPP3CB independent of E3 ligase activity, and their binding affinity was significantly enhanced in response to LLOMe treatment (Figure 7A, B Figure S5A-C). Consistently, LGALS3 was also required for the interaction of SMURF1 and PPP3CB evidenced by knocking down LGALS3 diminished the co-IP of SMURF1 and PPP3CB (Figure 7C). Again, overexpression of LGALS3 significantly increased their binding affinity in response to LLOMe (Figure 7D), suggesting LGALS3 might help to stabilize the interaction between SMURF1 and PPP3CB. Next, we mapped the specific interaction domain of SMURF1 and PPP3CB, and identified SMURF1 C2 domain directly interacted with CD domain of PPP3CB (Figure 7E-G), further strengthening the previous finding that the interconnected role of SMURF1 in regulating PPP3CB. It is reported that intracellular calcium controls PPP3/calci-neurin phosphatase activity by inducing the release of autoinhibitory AID from the CD domain [35]. Given that SMURF1 interacted with the CD domain of PPP3CB, we next explored whether SMURF1 affected the association between CD and AID domain of PPP3CB. Overexpression of SMURF1 or LGALS3 or treatment of LLOMe could completely release the inhibitory effect of AID from CD domain of PPP3CB (Figure 7H, Figure S5D). Strikingly, our data showed that deletion of SMURF1 promoted the binding, and LGALS3 overexpression rescued the disassociation (Figure 7I), and LGALS3 deletion could reverse the disassociation of AID from CD of PPP3CB in SMURF1-overexpressed cells (Figure 7J). Altogether, SMURF1 directly interacted with PPP3CB for the disassociation of AID from CD domain (Figure 7K).

LGALS3-SMURF1-PPP3CB complex stabilizes TFEB

Based on the above results, we hypothesized that LLOMe was connected to autophagy activation by facilitating LGALS3-SMURF1-PPP3CB recruitment to TFEB for its dephosphorylation. Interestingly, overexpression (or knock-down) of LGALS3 and PPP3CB together promoted (or decreased) the interaction affinity between SMURF1 and TFEB, emphasizing the importance of LGALS3-SMURF1-PPP3CB complex as a unit in stabilizing its interaction with TFEB (Figure 8A, B). Next, we tried to figure out how LGALS3-SMURF1-PPP3CB complex regulates its association with TFEB. Previous studies demonstrate that PPP3CB interacts with and dephosphorylates TFEB. However, whether PPP3CB directly interacts with TFEB and the mapped binding domain

has remained elusive. We first screened the possible interacted partner of PPP3CB and found that LLOMe promoted the binding affinity of PPP3CB with LGALS3, SMURF1 and PPP3R1, but not TFEB (Figure 8C), further strengthening that lysosome damage promoted the formation of LGALS3-SMURF1-PPP3CB complex. We also showed that PPP3CB, but not LGALS3, directly interacted with TFEB (Figure 8D, E, Figure S6A). Additionally, it revealed that the AID domain of PPP3CB interacted with 444–476 amino acids of TFEB (Figure 8F–H, Figure S6B–D). Secondly, to identify whether SMURF1 or LGALS3 played a role in stabilizing the binding of PPP3CB and TFEB, interestingly, we found that suppression of SMURF1 decreased, while overexpression of both wild-type SMURF1 and SMURF1^{C699A} increased, the binding affinity of PPP3CB and TFEB (Figure 8I, J). Consistently, LGALS3 and PPP3R1 were required for binding of PPP3CB and TFEB evidenced by knocking down LGALS3 or PPP3R1 decreased, while overexpression of LGALS3 or PPP3R1 increased, the interaction of PPP3CB and TFEB (Figure 8K, L). Of note, we found that the enhanced PPP3CB and TFEB interaction mediated by SMURF1 overexpression was abolished by LGALS3 deletion (Figure 8M). Overall, these data strengthened our hypothesis that LGALS3 and SMURF1 contribute to PPP3CB from “close” to “open” form, which facilitates TFEB docking to the AID domain (Figure 8N).

Discussion

The regulation of autophagy is thought to be a homeostatic process, with a fast induction that relies on post-translational modification and protein-protein interaction events, to maintain the sustained biogenesis of autophagic machinery that is mediated by transcriptional mechanisms [6,36]. Our results uncovered the role of SMURF1 as a regulator of the lysosomal system acting upstream of autophagy induction. The underlying regulatory circuitry is based on SMURF1 interactors (LGALS3 and PPP3/calci-neurin), whereby LGALS3-SMURF1-PPP3/calci-neurin acts as a central regulatory platform. This study also unveiled a hitherto unappreciated activation effect of PPP3/calci-neurin activity is not limited to starvation but also to damaged lysosome. The action of SMURF1 extends to its partner PPP3CB, a phosphatase that promotes TFEB translocation to the nucleus, where TFEB initiates the lysosomal transcriptional program. A physical link between PPP3/calci-neurin and TFEB is amplified by three factors: LGALS3, which is known to recruit members of the PPP3CB; SMURF1, which interacts with PPP3CB and PPP3R1. These protein interactions underlie the mechanism (Figure 9) that endomembrane damage not only prohibits MTORC1 signaling but also activates PPP3/calci-neurin signaling pathway mediated by SMURF1.

Previous reports established that MTOR kinase plays a key role in the promotion of cell growth in response to growth factors and amino acids. The essential role of the Ragulator-RRAG complex is to serve as an amino acid-regulated docking site for MTORC1 on lysosomal membranes [37]. The accumulation of amino acids inside the lysosomal lumen generates an activating signal that is transmitted to the RRAG GTPases via the V-ATPase-Ragulator interaction. In turn, the RRAGs

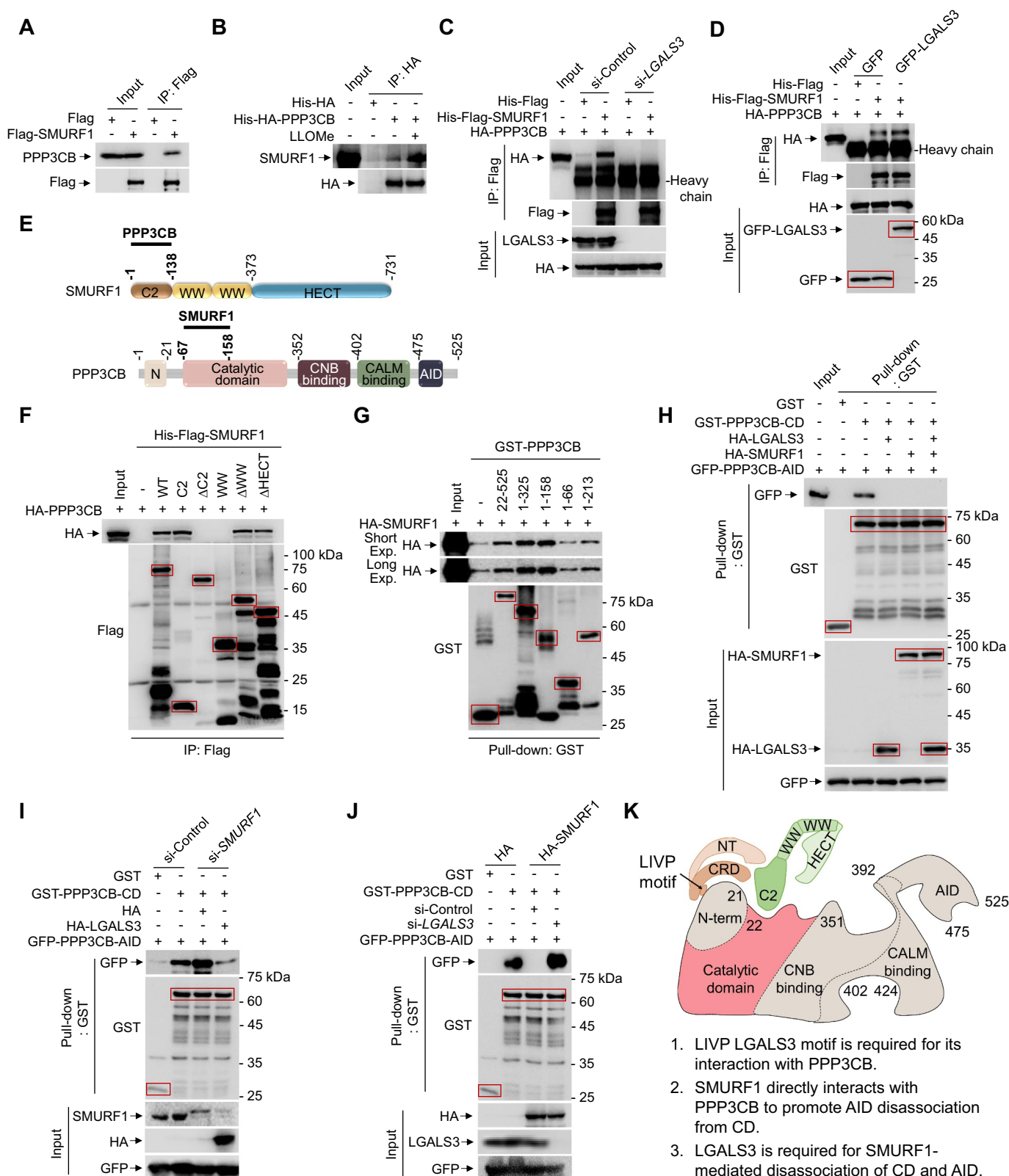


Figure 7. SMURF1 promotes PPP3CB CD and AID domain disassociation. (A) HEK293 cells were transfected with Flag or Flag-SMURF1 for 24 h. Co-IP analysis of the indirect association between Flag-SMURF1 and endogenous PPP3CB. (B) Co-IP analysis of the indirect association between His-HA-PPP3CB purified from *E. coli* and endogenous SMURF1 in HEK293 cells after the treatment of LLOMe (1 mM, 2 h) or DMSO. (C) HEK293 cells were transfected with LGALS3 or scramble siRNA oligos for 48 h, and then overexpressed with HA-PPP3CB for another 24 h. Co-IP analysis of the indirect association between HA-PPP3CB and His-Flag-SMURF1 purified from *E. coli*. (D) HA-PPP3CB-overexpressed HEK293 cells were transfected with GFP or GFP-LGALS3 for 24 h. Co-IP analysis of the indirect association between HA-PPP3CB and His-Flag-SMURF1 purified from *E. coli*. (E) Schematic diagram of mapping the direct association between SMURF1 and PPP3CB. (F) Co-IP analysis of the association between HA-PPP3CB expressed in HEK293 cells and His-Flag-SMURF1 constructs purified from *E. coli*. (G) GST affinity-isolation analysis of the association between HA-SMURF1 expressed in HEK293 cells and GST-PPP3CB constructs purified from *E. coli*. (H) GFP-PPP3CB-AID-overexpressed HEK293 cells were transfected with or without HA-SMURF1 (and/or HA-LGALS3) for 24 h. GST affinity-isolation analysis of the association between GFP-PPP3CB-AID and GST-PPP3CB-CD purified from *E. coli*. (I) HEK293 cells were transfected with SMURF1 or scramble siRNA oligos for 48 h, and then overexpressed with GFP-PPP3CB-AID, and with HA or HA-

physically recruit MTORC1 to the lysosomal surface [38]. Thus, MTORC1 exerts its activity on the lysosomal surface and is positively regulated by lysosomal nutrients. In addition, it has been well established that autophagy is negatively regulated by the MTOR kinase [39]. TFEB activity is regulated by MTORC1, which is the major kinase complex to phosphorylate TFEB (S211) and keep TFEB inactive in the cytoplasm by binding with the cytosolic chaperone YWHA/14-3-3 [14]. Yoshimori *et al.* reported that lysosomal damage selectively impairs the MTORC1-mediated phosphorylation of TFEB in an RAG GTPase and ATG conjugation system-dependent manner evidenced by that LLOMe treatment reduced TFEB S211 phosphorylation and YWHA/14-3-3 binding [27]. Our data also showed that LLOMe decreased phosphorylation of the MTORC1 substrate RPS6KB1/p70S6K. We previously reported that SMURF1 overexpression increases the phosphorylation of the MTORC1 substrate RPS6KB1/p70S6K by ubiquitinated degradation of PI3K-AKT-MTOR negative regulator PTEN [22,40]. We noticed that the SMURF1 overexpression promotes, but LLOMe (even though with SMURF1 overexpression) inhibits, MTOR activation measured by canonical substrates RPS6KB1/p70S6K. Interestingly, LLOMe treatment diminished the effect of SMURF1 overexpression in the phosphorylation of the MTORC1 substrate RPS6KB1/p70S6K (Figure 3A), suggesting lysosomal damage overrides the effect of SMURF1 overexpression on MTORC1 activity. We postulate that LLOMe-induced lysosome biogenesis led to dephosphorylation of TFEB by both affecting MTOR signaling and LGALS3-SMURF1-PPP3/calcineurin pathway.

Previously, lysosomal calcium release through MCOLN1 by starvation was a well-established requirement for locally induced PPP3/calcineurin activation. This leads to dephosphorylated TFEB, which is free to travel to the nucleus and induce the expression of lysosomal and autophagic genes [2,41]. It also implicated PPP3/calcineurin in a variety of both physiological and pathological processes, such as neuronal synaptic transmission, adaptive immune response and muscle remodeling after physical exercise [2,41]. However, it is still unclear whether and how PPP3/calcineurin activates TFEB in response to LLOMe. In this study, we identified that LGALS3-SMURF1-PPP3CB complex may recruit S211 phosphorylated TFEB to facilitate its dephosphorylation by PPP3CB. Whether lysosomal calcium efflux triggers SMURF1-PPP3/calcineurin system-dependent TFEB activation remains unknown. We first identified that MCOLN1-mediated calcium release is required for activation of SMURF1-PPP3/calcineurin pathway. Moreover, SMURF1-depleted cells exhibited impaired TFEB nuclear translocation following ML-SA1 treatment in response to LLOMe (Figure S2A), indicating agonist of MCOLN1 cannot override the silencing of SMURF1 during LLOMe treatment. Although it is still unknown at present how Ca^{2+} flux impacts SMURF1-mediated TFEB activation, our studies suggest that SMURF1-

mediated TFEB activation is particularly important after ESCRT repairing the ruptured lysosomes.

Importantly, we show a model representing how lysosome damages regulate TFEB by utilizing PPP3/calcineurin pathway. In our study, we found a small amount of LGALS3 puncta had been noticed in SMURF1-knocked-down cells before LLOMe treatment (Figure 1F), this may indicate that SMURF1 is required for maintaining lysosome integrity by eliminating spontaneously damaged lysosome. Previously, the peak times of the following proteins LGALS3 [24] (peak at 30 min-1 h after damage), TFEB [27] (3-6 h) and LC3 [27] (6-10 h) were different during the lysosomal damage response. Time-course experiments also revealed SMURF1 was already detectable before 1 h-treatment of LLOMe (Figure 1K). We speculated, during sustained lysosomal injury, SMURF1 is involved in ESCRT- and/or galectins-induced autophagy to remove damaged lysosomes (started at 1-2 h) and activate their biogenesis. Importantly, we also unveiled that SMURF1 plays a regulatory node role in how PPP3/calcineurin is orchestrated with endomembrane galectins and TFEB at the molecular level. PPP3CB normally stays in inactive status by autoinhibitory AID closing its catalytic domain [42]. LGALS3 recruits SMURF1 and PPP3CB into damaged lysosomal membrane. SMURF1 plays the role to disassociate the AID from the CD of PPP3CB. Thus, TFEB can be imported to nucleus by directly interacting with PPP3CB. So far, the transcription factors of the NFAT family, master regulators of T-cell activation, and TFEB, a master controller of autophagy, have been considered the main transcriptional mediators of PPP3/calcineurin function [43-45]. Of note, SMURF1 is required for TFEB nuclear import and activation physiologically. However, overexpression of SMURF1 was found in many types of tumors and correlated with the patient's survival rate [22]. We noticed the interesting finding that SMURF1 overexpression does not localize on lysosomes, but still can induce TFEB nuclear translocation, indicating overexpression of SMURF1 may override the calcium release to activate TFEB in a calcium-independent manner. Further study needs to verify whether SMURF1 could interact and/or ubiquitylate TFEB. We also hypothesize that overexpression of SMURF1 rewires the constitutive autophagic machinery in response to environmental damage, which may account for tumorigenesis in lysosomal-dependent and independent manner. Thus, the discovery that SMURF1 is a PPP3/calcineurin central regulation platform expands the current view on immunometabolism and associated innate T cell responses and tumorigenesis. In addition, autophagy machinery, such as GABARAPs (the gamma-aminobutyric acid receptor-associated proteins), can also work upstream of TFEB [1,27,46]. Our data also revealed a positive feedback loop that SMURF1 activates TFEB, which also can stabilize the PPP3/calcineurin complex (data not shown). This

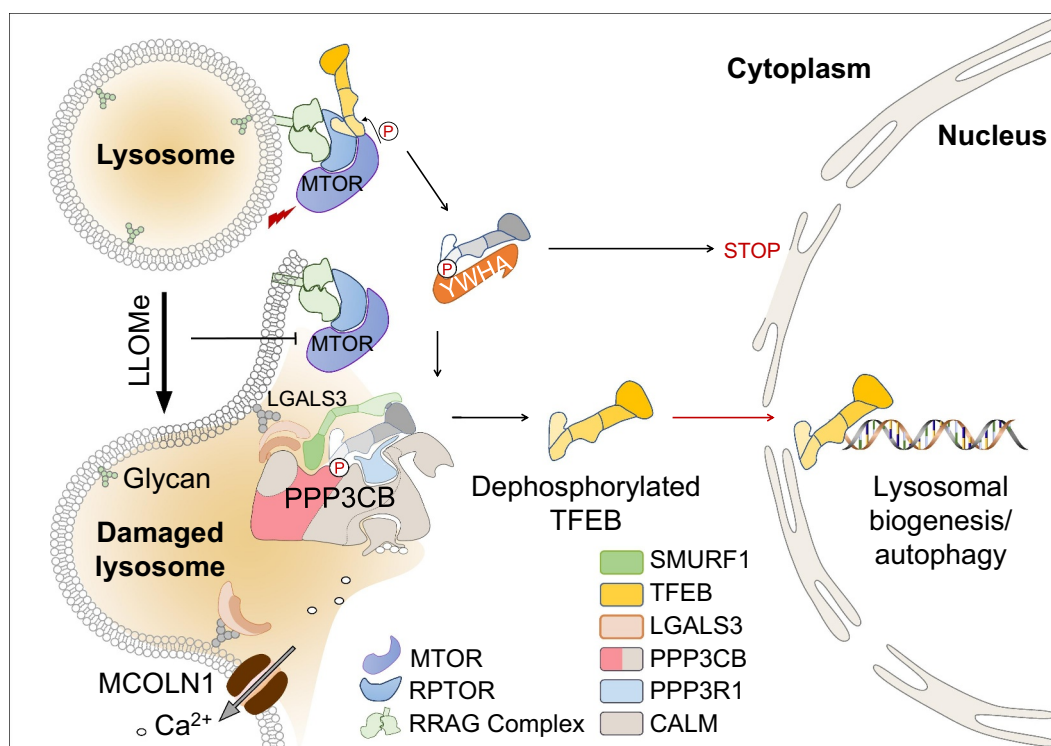


Figure 9. SMURF1 controls PPP3/calcineurin to drive TFEB nuclear translocation through its dephosphorylation. A schematic diagram of SMURF1 controls the formation of PPP3/calcineurin complex and TFEB activation. PPP3CB stays in inactive status by autoinhibitory AID domain closed its catalytic domain. LGALS3 recruits SMURF1 and PPP3CB into the damaged lysosomal membrane. SMURF1 disassociates the AID from the CD domain of PPP3CB. PPP3R1 interacts with and stabilizes the TFEB conformation to enhance the dephosphorylation efficiency of TFEB.

relationship fits the general biological principle of feedback control, whereby SMURF1-mediated TFEB nuclear import may cooperate with autophagy machinery in positive feedback for damaged lysosomal clearance and biogenesis.

In conclusion, the identification of a mechanism by which SMURF1 regulates autophagy through the activation of the phosphatase PPP3/calcineurin and the transcription factor TFEB further supports the role of the lysosome as a signaling hub. In summary, SMURF1 controls the key regulator of lysosomal biogenesis, whereas SMURF1 together with LGALS3 and PPP3/calcineurin governs nearly all stages of the autolysosome pathway. Hence, a subset of SMURF1 indirectly acts to complete the autophagy pathway to exert its function on autophagosome maturation by regulating TFEB. The molecular complexes formed by SMURF1 participate in cellular responses to infectiousness and LLOMe. With many functions converging on SMURF1, as shown here and elsewhere, it is not surprising that SMURF1 has emerged as a medically important locus. Thus, SMURF1 and its complexes, as the functions of SMURF1 uncovered here, should be considered as potential drug targets.

Materials and methods

Cell culture, transfection, and drug treatment

The HEK293T (human embryonic kidney cell line) was purchased from American Type Culture Collection (CRL-3216), and the HEK293A cell line was purchased from Invitrogen (R70507). Cells were cultured at 37°C, 5% CO₂ atmosphere in DMEM (Dulbecco's Modified Eagle's Medium; Servicebio, G4511) supplemented with 10% FBS (fetal bovine serum) and 1% penicillin-streptomycin (1 × 10⁴ units/mL penicillin; 1 × 10⁴ µg/mL streptomycin). Cells were transfected with indicated plasmids using polyethylenimine (PEI; Polysciences 23,966-1) according to the manufacturer's instructions. For siRNA (small interfering RNA) transfection, cell suspension was treated with siRNA or scramble siRNA and lipofectamine RNAiMax Reagent (Invitrogen 13,778-150) according to the manufacturer's instructions.

Cells were treated with LLOMe (GLPBIO, GA22634), bafilomycin A₁ (Selleck, S1413), MG132 (MCE, HY-13258), torin1 (Tocris Bioscience, 4247), CsA (Aladdin, C106893),

Flag-PPP3CB purified from *E. coli*. (E) Co-IP analysis of the direct interaction between His-HA-TFEB and His-Flag-PPP3CB purified from *E. coli*. (F) Schematic diagram of mapping the interaction between TFEB and PPP3CB. (G) Co-IP analysis of the indirect interaction between HA-PPP3CB expressed in HEK293 cells and GST-TFEB constructs purified from *E. coli*. (H) Co-IP analysis of the direct interaction between His-HA-TFEB and GST-PPP3CB constructs purified from *E. coli*. (I) HEK293 cells were transfected with *SMURF1* or scramble siRNA oligos for 48 h, and then overexpressed with GFP-TFEB for another 24 h. Co-IP analysis of the indirect association between GFP-TFEB and His-Flag-PPP3CB purified from *E. coli*. (J) HEK293 cells were transfected with GFP-TFEB and HA, HA-SMURF1 or HA-SMURF1^{C699A} for 24 h. Co-IP analysis of the indirect association between GFP-TFEB and His-Flag-PPP3CB purified from *E. coli*. (K) HEK293 cells were transfected with *LGALS3*, *PPP3R1* or scramble siRNA oligos for 48 h, and then overexpressed with GFP-TFEB for another 24 h. Co-IP analysis of the indirect association between GFP-TFEB and His-Flag-PPP3CB purified from *E. coli*. (L) HEK293 cells were transfected with GFP-TFEB and HA-*LGALS3* or HA-*PPP3R1* or HA for 24 h. Co-IP analysis of the indirect association between GFP-TFEB and His-Flag-PPP3CB purified from *E. coli*. (M) HEK293 cells were transfected with *LGALS3* or scramble siRNA oligos for 48 h, and then overexpressed with GFP-PPP3CB and HA or HA-SMURF1 for another 24 h. Co-IP analysis of the indirect association between GFP-PPP3CB and His-Flag-TFEB purified from *E. coli*. (N) Schematic diagram of PPP3R1 interacts with TFEB and LGALS3-SMURF1-PPP3CB complex.

ML-SA1 (TargetMol 332,382-54-4), BAPTA-AM (TargetMol, T6245) and DMSO (Solarbio, D8371).

Antibodies

The antibodies used for western blot, immunofluorescence and immunoprecipitation were: anti-Flag (Sigma, F3165), anti-Flag (Cell Signaling Technology, 14,793), anti-GST (Sigma, G1160), anti-GST (ABclonal, AE001), anti-GST (proteintech, 66,001-2-Ig), anti-His (abcam, ab18184), anti-His (proteintech 66,005-1-Ig), anti-His (ABclonal, AE012), anti-GFP (proteintech, 66,002-1-Ig), anti-HA (MBL, M180-3), anti-ACTB/ β -actin (Sigma, A1978), anti-H2B/histone 2B (Santa Cruz Biotechnology, sc-515,808), anti-SMURF1 (Santa Cruz Biotechnology, sc-100,616), anti-SMURF1 (abcam, ab57573), anti-SMURF1 (abcam, ab236081), anti-TFEB (Cell Signaling Technology, 37,785), anti-TFEB (abcam, ab220695), anti-TFEB (proteintech, 13,372-1-AP), anti-MCOLN1/mucolipin 1 (Invitrogen, PA146474), anti-PPP3CB (proteintech, 13,340-1-AP), anti-PPP3R1 (proteintech, 13,210-1-AP), anti-LC3B (Novus Biologicals, NB100-2220), anti-LC3B (Sigma, L7543), anti-LAMP2 (RD systems, MAB6228), anti-LAMP2 (Santa Cruz Biotechnology, sc-20,004), anti-LAMP1 (Cell Signaling Technology, 9091), anti-ubiquitin (MBL, D058-3), anti-ubiquitin (ABclonal, A19686), anti-SQSTM1/p62 (Enzo life science, BML-PW9860), anti-SQSTM1/p62 (MBL, PM045), anti-SQSTM1/p62 (MBL, M162-3), anti-LGALS3 (Cell Signaling Technology, 87,985), anti-LGALS3 (abcam, ab2785), anti-LGALS3 (proteintech, 60,207-1-Ig), anti-LGALS8 (ABclonal, A6646).

The secondary antibodies for western blot: goat anti-mouse IgG (BOSTER, BA1050), goat anti-rabbit IgG (BOSTER, BA1054), rabbit anti-rat IgG (BOSTER, BA1058), rabbit anti-mouse IgG light chain (Cell Signaling Technology 58,802), rabbit anti-rabbit IgG light chain (Cell Signaling Technology 45,262), goat anti-mouse IgG light chain (ABclonal, AS062).

The secondary antibodies for immunofluorescence: Alexa Fluor® 488 goat anti-mouse IgG (Thermo Fisher Scientific, A11001), Alexa Fluor® 488 goat anti-rabbit IgG (Thermo Fisher Scientific, A11008), Alexa Fluor® 555 goat anti-mouse IgG (Thermo Fisher Scientific, A21425), Alexa Fluor® 555 goat anti-rabbit IgG (Thermo Fisher Scientific, A21428), goat anti-rabbit IgG H&L (Alexa Fluor 405) (abcam, ab175652), goat anti-mouse IgG H&L (Alexa Fluor 647) (abcam, ab150115). Seal the coverslip with mounting medium with DAPI (4',6-diamidino-2-phenylindole) (abcam, ab104139).

Western blot

Western blot was used to detect the protein expression. The collected cells were lysed with RIPA buffer supplemented with phosphatase inhibitor (BOSTER, AR1195) and 1 mM phenylmethanesulfonyl fluoride (PMSF; BOSTER, AR0162) and boiled with 5× loading buffer. The proteins were separated on SDS-PAGE (sodium dodecyl sulfate polyacrylamide gel electrophoresis) and transferred to a nitrocellulose membrane, and then blocked with 5% nonfat dry milk at room temperature for 1 h and subsequently incubated with the primary antibody overnight at 4°C. The nitrocellulose membranes

were washed three times with TBST (Tris buffered saline with Tween) (0.1% Tween-20 [Solarbio, T8220] in TBS [Tris buffered saline; 0.1 M Tris, 1.5 M NaCl, pH 8.0]) and incubated with horseradish peroxidase (HRP)-conjugated secondary antibodies (proteintech, SA00001-1). After washing with 0.1% TBST, the protein signals were visualized by ECL (enhanced chemiluminescence) according to the manufacturer's instructions.

Immunofluorescence and live cell staining

The cells were seeded onto a glass slide in 12-well plates at a density of 1×10^5 cells/well. At the end of treatment, cells were fixed with 4% paraformaldehyde for 15 min and then permeated with 0.1% Triton X-100 (Coolaber, CT11451) in phosphate-buffered saline (PBS; Servicebio, G0002) for 5 min at room temperature. Subsequently, cells were blocked with 1% bovine serum albumin (BSA; Solarbio, A8020; Servicebio, GC305010) at room temperature for 1 h and then incubated with antibody diluent (antibodies in PBS) at 4°C overnight. After that, the cells were incubated at room temperature with fluorescence secondary antibody for 1 h and washed with 0.1% Tween-20-PBS (PBST) three times later. Finally, DAPI diluted solution was added to staining for 10 min in the dark. The images were acquired by confocal laser scanning microscope (Nikon) after the slides were sealed with anti-fluorescence quenching sealing agent, and the ImageJ software was applied to quantify the intensity of fluorescence. LysoTracker (abcam, ab176827) and Hoechst (aladdin, H422767) were used for living cells staining for 10 min.

Nuclear and cytoplasmic separation

Cells were collected and the total cell lysates were produced by 160 μ L Buffer A (10 mM N-2-hydroxyethylpiperazine-N-ethane-sulphonic acid [HEPES], pH 7.9, 10 mM KCl, 1 mM ethylenediaminetetraacetic acid [EDTA], 1 mM ethylene glycol tetraacetic acid [EGTA], 1 mM dithiothreitol [DTT]) containing 100 mM PMSF, 100 mM phosphatase inhibitors and 0.5% NP-40 (Solarbio, N8030). 80 μ L cell lysates were taken out for total and the rest was incubated on ice for another 30 min. The rest cell lysates were centrifuged at 600× g for 15 min. The supernatants were cytoplasmic fraction and the precipitates were nuclear fraction separately. The nuclear fraction was washed three times with 200 μ L Buffer A. Added 80 μ L Buffer C (20 mM HEPES, pH 7.9, 400 mM KCl, 1 mM EDTA, 1 mM EGTA, 1 mM DTT) containing 100 mM PMSF and 100 mM phosphatase inhibitors to the pellet. Vortexed on the highest setting for 15 s and incubated at 4°C for 30 min. Centrifuged at 10,000× g for 5 min and collected the supernatant to obtain the nuclear fraction.

Recombinant protein purification

Escherichia coli BL21 (DE3) was transformed with indicated recombinant plasmids or empty plasmids and cultured at 37°C in Luria-Bertani medium supplemented with ampicillin (50 μ g/mL, Coolaber, CA2031) until the OD (optical density, 600 nm) reached to 0.5-0.7. Then IPTG

(isopropyl β -D-thiogalactopyranoside, 1 mM for 4 h; Sigma, I5502) was added to *Escherichia coli* BL21 to induce the expression of recombinant proteins. Finally, His-tagged proteins and glutathione-S-transferase (GST)-tagged proteins were respectively affinity purified using ProBond™ Purification System (Invitrogen, K85001) and glutathione-agarose beads (Solarbio, P2020) according to the manufacturer's protocols. The efficiency of purified recombinant proteins was analyzed by SDS-PAGE.

Affinity-isolation

The bacterial-expressed purified GST-tagged proteins were incubated with glutathione-agarose beads for 4 h at 4°C. After incubation, the beads were washed with cold 1× PBS at 3000× g for 2 min 6 times at 4°C, and then incubated with the second protein for 4 h at 4°C. After incubation, the beads were washed with PBS at 3000× g for 2 min 6 times at 4°C. Finally, the proteins were eluted with 2× loading buffer and analyzed by western blotting.

Immunoprecipitation

The rProtein G beads (Solarbio, R8300) were incubated with the indicated antibody for 4 h at 4°C. First, the beads were washed with cold 1× PBS at 3000× g for 2 min 6 times at 4°C. Second, the beads with antibodies were incubated with proteins from transfected native cell lysates (or bacterial-expressed negative control and targeted proteins) for 4 h at 4°C, respectively. Then the beads were washed with cold 1× PBS at 3000× g for 2 min 6 times at 4°C, and incubated with equally divided bacterial-expressed proteins (or indicated native cell lysates) for 4 h at 4°C. The beads were washed with cold 1× PBS at 3000× g for 2 min 6 times at 4°C, then the proteins were eluted with 2× loading buffer and separated by western blotting.

Ex vivo immunoprecipitation (IP): The immunoprecipitation with purified protein A in the expression system and the cell lysates containing protein B in the cell culture was conducted to verify the indirect interaction between protein A and protein B; *In vitro* IP: The immunoprecipitation with purified protein A and protein B in the expression system respectively was conducted to verify the direct interaction.

Ethical profiles for experiment

This study did not involve human or animal experiments.

Statistical analysis

All experiments were repeated two to three times with the indicated numbers of cells. Data are presented as mean \pm SEM. Statistical significance was determined using the unpaired two-tailed Student's t-test. For imaging analysis, two-tier tests were used to first combine technical replicates and then evaluate biological replicates. * $p < 0.05$; ** $p < 0.01$; *** $p < 0.001$; NS, not significant.

Acknowledgements

We thank the Collaborative Research Fund of Chinese Institute for Brain Research, Beijing (No: 2021-NKX-XM-06); the Biological and Medical Engineering Core Facilities of Beijing Institute of Technology for supporting experimental equipments, Chao Yang for valuable help with confocal microscopy technical support; and Mu Ma from Yew Wah International Education School for providing us art design guidance for schematic diagram.

Disclosure statement

No potential conflict of interest was reported by the authors.

Funding

This work was supported by the National Natural Science Foundation of China [U21A20200], The Natural Science Foundation of Beijing Municipality [Z190018], and the National Natural Science Foundation of China [81870123].

Data availability statement

These datasets can be accessed on request from Lei Dong; Key Laboratory of Molecular Medicine and Biological Diagnosis and Treatment (Ministry of Industry and Information Technology), School of Life Science, 5th South Zhongguancun Street, Haidian District, Beijing Institute of Technology, Beijing, China. Email: ldong@bit.edu.cn.

ORCID

Lei Dong  <http://orcid.org/0000-0001-7530-7427>

References

- [1] Mizushima N, Levine B, Cuervo AM, et al. Autophagy fights disease through cellular self-digestion. *Nature*. 2008;451(7182):1069–1075. doi: 10.1038/nature06639
- [2] Medina DL, Di Paola S, Peluso I, et al. Lysosomal calcium signaling regulates autophagy through calcineurin and TFEB. *Nat Cell Biol*. 2015;17(3):288–299. doi: 10.1038/ncb3114
- [3] Dong L, Liu L, Li Y, et al. E3 ligase Smurf1 protects against misfolded SOD1 in neuronal cells by promoting its K63 ubiquitylation and aggresome formation. *Hum Mol Genet*. 2022;31(12):2035–2048. doi: 10.1093/hmg/ddac008
- [4] Franco LH, Nair VR, Scharn CR, et al. The ubiquitin ligase Smurf1 functions in selective autophagy of Mycobacterium tuberculosis and anti-tuberculous host defense. *Cell Host Microbe*. 2017;21:59–72. doi: 10.1016/j.chom.2016.11.002
- [5] Shariq M, Quadir N, Alam A, et al. The exploitation of host autophagy and ubiquitin machinery by Mycobacterium tuberculosis in shaping immune responses and host defense during infection. *Autophagy*. 2022;19:1–21. doi: 10.1080/15548627.2021.2021495
- [6] Settembre C, Di Malta C, Polito VA, et al. TFEB links autophagy to lysosomal biogenesis. *Science*. 2011;332(6036):1429–1433. doi: 10.1126/science.1204592
- [7] Raben N, Puertollano R. TFEB and TFE3: linking lysosomes to cellular adaptation to stress. *Annu Rev Cell Dev Biol*. 2016;32:255–278. doi: 10.1146/annurev-cellbio-111315-125407
- [8] Zhou J, Li X-Y, Liu Y-J, et al. Full-coverage regulations of autophagy by ROS: from induction to maturation. *Autophagy*. 2022;18:1240–1255. doi: 10.1080/15548627.2021.1984656
- [9] Kim S, Lee J-Y, Shin SG, et al. ESRR α (estrogen related receptor alpha) is a critical regulator of intestinal homeostasis through activation of autophagic flux via gut microbiota. *Autophagy*. 2021;17:2856–2875. doi: 10.1080/15548627.2020.1847460
- [10] Najibi M, Honwad HH, Moreau JA, et al. A novel Nox/Phox-Cd38-naadp-tfeb axis important for macrophage activation

- during bacterial phagocytosis. *Autophagy*. 2022;18:124–141. doi: [10.1080/15548627.2021.1911548](https://doi.org/10.1080/15548627.2021.1911548)
- [11] Schuster EM, Epple MW, Glaser KM, et al. TFEB induces mitochondrial itaconate synthesis to suppress bacterial growth in macrophages. *Nat Metab*. 2022;4:856–866. doi: [10.1038/s42255-022-00605-w](https://doi.org/10.1038/s42255-022-00605-w)
 - [12] Perera RM, Stoykova S, Nicolay BN, et al. Transcriptional control of autophagy-lysosome function drives pancreatic cancer metabolism. *Nature*. 2015;524:361–365. doi: [10.1038/nature14587](https://doi.org/10.1038/nature14587)
 - [13] Roczniaik-Ferguson A, Petit CS, Froehlich F, et al. The transcription factor TFEB links mTORC1 signaling to transcriptional control of lysosome homeostasis. *Sci Signal*. 2012;5:ra42. doi: [10.1126/scisignal.2002790](https://doi.org/10.1126/scisignal.2002790)
 - [14] Martina JA, Chen Y, Gucek M, et al. mTORC1 functions as a transcriptional regulator of autophagy by preventing nuclear transport of TFEB. *Autophagy*. 2012;8:903–914. doi: [10.4161/auto.19653](https://doi.org/10.4161/auto.19653)
 - [15] Jeong SJ, Stitham J, Evans TD, et al. Trehalose causes low-grade lysosomal stress to activate TFEB and the autophagy-lysosome biogenesis response. *Autophagy*. 2021;17:3740–3752. doi: [10.1080/15548627.2021.1896906](https://doi.org/10.1080/15548627.2021.1896906)
 - [16] Kingsbury TJ, Cunningham KW. A conserved family of calcineurin regulators. *Genes Dev*. 2000;14(13):1595–1604. doi: [10.1101/gad.14.13.1595](https://doi.org/10.1101/gad.14.13.1595)
 - [17] Valdor R, Mocholi E, Botbol Y, et al. Chaperone-mediated autophagy regulates T cell responses through targeted degradation of negative regulators of T cell activation. *Nat Immunol*. 2014;15:1046–1054. doi: [10.1038/ni.3003](https://doi.org/10.1038/ni.3003)
 - [18] De Windt LJ, Lim HW, Bueno OF, et al. Targeted inhibition of calcineurin attenuates cardiac hypertrophy in vivo. *Proc Natl Acad Sci U S A*. 2001;98:3322–3327. doi: [10.1073/pnas.031371998](https://doi.org/10.1073/pnas.031371998)
 - [19] Taigen T, De Windt LJ, Lim HW, et al. Targeted inhibition of calcineurin prevents agonist-induced cardiomyocyte hypertrophy. *Proc Natl Acad Sci U S A*. 2000;97:1196–1201. doi: [10.1073/pnas.97.3.1196](https://doi.org/10.1073/pnas.97.3.1196)
 - [20] Kafadar KA, Zhu H, Snyder M, et al. Negative regulation of calcineurin signaling by Hrr25p, a yeast homolog of casein kinase I. *Genes Dev*. 2003;17:2698–2708. doi: [10.1101/gad.1140603](https://doi.org/10.1101/gad.1140603)
 - [21] Zhang Y, Liu R-B, Cao Q, et al. USP16-mediated deubiquitination of calcineurin controls peripheral T cell maintenance. *J Clin Invest*. 2019;129:2856–2871. doi: [10.1172/JCI123801](https://doi.org/10.1172/JCI123801)
 - [22] Xia Q, Zhang H, Zhang P, et al. Oncogenic Smurf1 promotes PTEN wild-type glioblastoma growth by mediating PTEN ubiquitylation. *Oncogene*. 2020;39:5902–5915. doi: [10.1038/s41388-020-01400-1](https://doi.org/10.1038/s41388-020-01400-1)
 - [23] Jia J, Abudu YP, Claude-Taupin A, et al. Galectins control mTOR in response to endomembrane damage. *Mol Cell*. 2018;70:120–135 e128. doi: [10.1016/j.molcel.2018.03.009](https://doi.org/10.1016/j.molcel.2018.03.009)
 - [24] Jia J, Claude-Taupin A, Gu Y, et al. Galectin-3 coordinates a cellular system for lysosomal repair and removal. *Dev Cell*. 2020;52:69–87 e68. doi: [10.1016/j.devcel.2019.10.025](https://doi.org/10.1016/j.devcel.2019.10.025)
 - [25] Chauhan S, Kumar S, Jain A, et al. Trims and galectins Globally Cooperate and TRIM16 and galectin-3 Co-direct autophagy in endomembrane damage homeostasis. *Dev Cell*. 2016;39:13–27. doi: [10.1016/j.devcel.2016.08.003](https://doi.org/10.1016/j.devcel.2016.08.003)
 - [26] Watson RO, Manzanillo PS, Cox JSE. Tuberculosis DNA targets bacteria for autophagy by activating the host DNA-sensing pathway. *Cell*. 2012;150:803–815. doi: [10.1016/j.cell.2012.06.040](https://doi.org/10.1016/j.cell.2012.06.040)
 - [27] Nakamura S, Shigeyama S, Minami S, et al. LC3 lipidation is essential for TFEB activation during the lysosomal damage response to kidney injury. *Nat Cell Biol*. 2020;22:1252–1263. doi: [10.1038/s41556-020-00583-9](https://doi.org/10.1038/s41556-020-00583-9)
 - [28] Gatica D, Lahiri V, Klionsky DJ. Cargo recognition and degradation by selective autophagy. *Nat Cell Biol*. 2018;20:233–242. doi: [10.1038/s41556-018-0037-z](https://doi.org/10.1038/s41556-018-0037-z)
 - [29] Orvedahl A, Sumpter R, Xiao G, et al. Image-based genome-wide siRNA screen identifies selective autophagy factors. *Nature*. 2011;480:113–117. doi: [10.1038/nature10546](https://doi.org/10.1038/nature10546)
 - [30] Napolitano G, Di Malta C, Esposito A, et al. A substrate-specific mTORC1 pathway underlies Birt-Hogg-dubé syndrome. *Nature*. 2020;585:597–602. doi: [10.1038/s41586-020-2444-0](https://doi.org/10.1038/s41586-020-2444-0)
 - [31] Stewart AA, Ingebritsen TS, Manalan A, et al. Discovery of a Ca²⁺- and calmodulin-dependent protein phosphatase: probable identity with calcineurin (CaM-BP80). *FEBS Lett*. 1982;137(1):80–4. doi: [10.1016/0014-5793\(82\)80319-0](https://doi.org/10.1016/0014-5793(82)80319-0)
 - [32] Thurston TL, Wandel MP, von Muhlinen N, et al. Galectin 8 targets damaged vesicles for autophagy to defend cells against bacterial invasion. *Nature*. 2012;482:414–418. doi: [10.1038/nature10744](https://doi.org/10.1038/nature10744)
 - [33] Kilka S, Erdmann F, Migdoll A, et al. The proline-rich N-terminal sequence of calcineurin α determines substrate binding. *Biochemistry*. 2009;48:1900–1910. doi: [10.1021/bi8019355](https://doi.org/10.1021/bi8019355)
 - [34] Gal M, Li S, Luna RE, et al. The LxVP and PxIXIT NFAT motifs bind jointly to overlapping epitopes on calcineurin's catalytic domain distant to the regulatory domain. *Structure*. 2014;22:1016–1027. doi: [10.1016/j.str.2014.05.006](https://doi.org/10.1016/j.str.2014.05.006)
 - [35] Klee CB, Crouch TH, Krinks MH. Calcineurin: a calcium- and calmodulin-binding protein of the nervous system. *Proc Natl Acad Sci U S A*. 1979;76:6270–6273. doi: [10.1073/pnas.76.12.6270](https://doi.org/10.1073/pnas.76.12.6270)
 - [36] Hernandez GA, Perera RM. Autophagy in cancer cell remodeling and quality control. *Molecular Cell*. 2022;82:1514–1527. doi: [10.1016/j.molcel.2022.03.023](https://doi.org/10.1016/j.molcel.2022.03.023)
 - [37] Sancak Y, Bar-Peled L, Zoncu R, et al. Ragulator-rag complex targets mTORC1 to the lysosomal surface and is necessary for its activation by amino acids. *Cell*. 2010;141:290–303. doi: [10.1016/j.cell.2010.02.024](https://doi.org/10.1016/j.cell.2010.02.024)
 - [38] Zoncu R, Bar-Peled L, Efeyan A, et al. mTORC1 senses lysosomal amino acids through an inside-out mechanism that requires the vacuolar H⁺-ATPase. *Science*. 2011;334:678–683. doi: [10.1126/science.1207056](https://doi.org/10.1126/science.1207056)
 - [39] Liu GY, Sabatini D. M. mTOR at the nexus of nutrition, growth, ageing and disease. *Nat Rev Mol Cell Biol*. 2020;21:183–203. doi: [10.1038/s41580-019-0199-y](https://doi.org/10.1038/s41580-019-0199-y)
 - [40] Xia Q, Li W, Ali S, et al. Smurf1 silencing restores PTEN expression that ameliorates progression of human glioblastoma and sensitizes tumor cells to mTORC1/C2 inhibitor Torin1. *iScience*. 2021;24:103528. doi: [10.1016/j.isci.2021.103528](https://doi.org/10.1016/j.isci.2021.103528)
 - [41] Medina DL, Ballabio A. Lysosomal calcium regulates autophagy. *Autophagy*. 2015;11:970–971. doi: [10.1080/15548627.2015.1047130](https://doi.org/10.1080/15548627.2015.1047130)
 - [42] Kissinger CR, Parge HE, Knighton DR, et al. Crystal structures of human calcineurin and the human FKBP12–FK506–calcineurin complex. *Nature*. 1995;378:641–644. doi: [10.1038/378641a0](https://doi.org/10.1038/378641a0)
 - [43] Chapman NM, Boothby MR, Chi H. Metabolic coordination of T cell quiescence and activation. *Nat Rev Immunol*. 2020;20:55–70. doi: [10.1038/s41577-019-0203-y](https://doi.org/10.1038/s41577-019-0203-y)
 - [44] Zhang X, Yu L, Xu H. Lysosome calcium in ROS regulation of autophagy. *Autophagy*. 2016;12:1954–1955. doi: [10.1080/15548627.2016.1212787](https://doi.org/10.1080/15548627.2016.1212787)
 - [45] Kar P, Mirams GR, Christian HC, et al. Control of NFAT isoform activation and NFAT-Dependent gene expression through two coincident and spatially segregated intracellular Ca²⁺ signals. *Molecular Cell*. 2016;64:746–759. doi: [10.1016/j.molcel.2016.11.011](https://doi.org/10.1016/j.molcel.2016.11.011)
 - [46] Goodwin JM, Walkup WG, Hooper K, et al. GABARAP sequesters the FLCN-FNIP tumor suppressor complex to couple autophagy with lysosomal biogenesis. *Sci Adv*. 2021;7:eabj2485. doi: [10.1126/sciadv.abj2485](https://doi.org/10.1126/sciadv.abj2485)